ChemComm

COMMUNICATION

View Article Online
View Journal | View Issue

Cite this: *Chem. Commun.*, 2017, 53, 11465

Received 14th August 2017,
Accepted 2nd October 2017

DOI: 10.1039/c7cc06327j

rsc.li/chemcomm

Visible light-driven, magnetically steerable gold/iron oxide nanomotors†

Dekai Zhou,‡[ab] Liqiang Ren,‡[c] Yuguang C. Li,[b] Pengtao Xu,[b] Yuan Gao,[a] Guangyu Zhang,[a] Wei Wang,*[d] Thomas E. Mallouk*[b] and Longqiu Li*[a]

We report the synthesis and properties of rod-shaped gold/iron oxide nanomotors that are powered by visible light in dilute hydrogen peroxide solutions. Electrochemical measurements confirmed that the light-driven nanomotors operate by a self-electrophoretic mechanism, modulated by the photovoltage and the photoconductivity of gold/iron oxide. Due to the magnetism of iron oxide, the nanomotors can be steered by an external magnetic field without incorporating additional magnetic materials into the nanomotors.

Nano/micromotors are objects that locally convert energy from their surroundings into movement.[1,2] Autonomous nano/micromotors hold considerable promise for drug or cargo delivery,[3–6] minimally invasive surgery,[7,8] sensing,[9–11] micromachine assembly[12–14] and environmental monitoring and remediation.[15–18] The scientific community has witnessed an explosion of nanomotor-related research since the first bimetallic motors were described in 2004.[19] Chemical,[19,20] magnetic,[3,21–23] electrical,[24,25] acoustic,[4,12,26–29] and thermal[30,31] energy have been harnessed to power nano/micromotors, and their respective propulsion mechanisms have been studied extensively.[19,26,30,32] A desired feature, and thus a common goal among researchers, is to achieve propulsion that is biocompatible, highly energy efficient, and easy to apply and control. In pursuit of this goal, recent research has been devoted to light-driven motors.[33–39] By taking advantage of the photoelectric effect of semiconductors, light energy can be converted to chemical energy. Previously we reported visible light-driven Cu_2O–Au and Si–Au[40] micromotors that were fabricated by vapor deposition methods and propelled by self-electrophoresis. There remains room for improvement, particularly with regard to motor speed, response to visible light, and the ability to steer photochemically powered micromotors.

As a step towards these goals, we report here the template synthesis of gold/iron oxide nanomotors which show rapid motion at low concentrations of hydrogen peroxide under visible light illumination. By controlling the light intensity, the velocity of the nanomotors can be adjusted and they can be activated or stopped rapidly by switching the light on or off. Their axial motion can be steered by an externally applied magnetic field without the incorporation of ferromagnetic materials such as Ni due to the magnetism of nanoscale iron oxide particles. In addition, the nanomotors can be synthesized rapidly and inexpensively in scalable quantities by electrochemical deposition. Taken together these properties result in an improved class of light-driven nanomotors that are potentially useful in applications including drug delivery and environmental monitoring and remediation.

Gold/iron oxide nanorods were fabricated in anodic alumina (AAO) membranes by previously reported procedures as shown

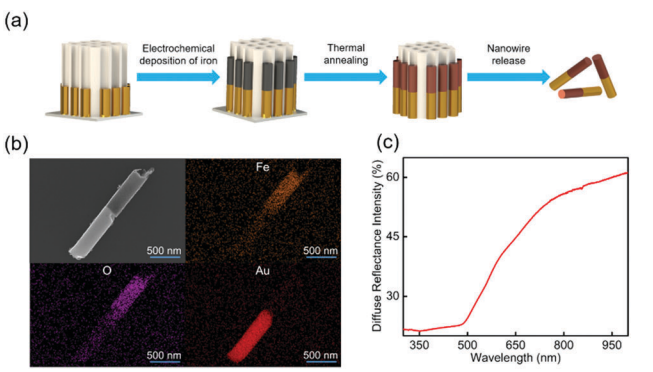

Fig. 1 (a) Electrodeposition of gold/iron oxide nanorods in anodic alumina membranes. (b) SEM and EDS analysis of gold/iron oxide nanorod. (c) Diffuse reflectance spectra of the iron oxide nanorods on a glass slide.

[a] *Key Laboratory of Microsystems and Microstructures Manufacturing, Harbin Institute of Technology, Harbin, Heilongjiang 150001, P. R. China. E-mail: longqiuli@hit.edu.cn*

[b] *Departments of Chemistry, Biochemistry and Molecular Biology and Physics, The Pennsylvania State University, University Park, PA 16802, USA. E-mail: tem5@psu.edu*

[c] *Department of Engineering Science and Mechanics, The Pennsylvania State University, University Park, PA 16802, USA*

[d] *School of Materials Science and Engineering, Harbin Institute of Technology, Shenzhen Graduate School, Shenzhen, Guangdong 518055, P. R. China*

† Electronic supplementary information (ESI) available: Videos, materials and methods, and characterization data, 2 pp. See DOI: 10.1039/c7cc06327j

‡ These authors contributed equally to this work.

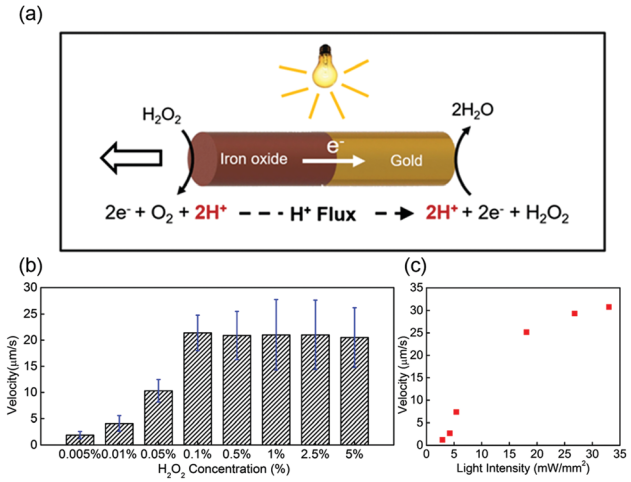

Fig. 2 (a) Illustration of the bipolar electrochemical propulsion mechanism of gold/iron oxide nanomotors activated by visible light in hydrogen peroxide solutions. (b) Speeds of the nanomotors at different hydrogen peroxide concentrations illuminated with light of 33 mW mm^{-2}. (c) Speed of a gold/iron oxide nanomotor illuminated at different light intensities in 2.5 v% hydrogen peroxide solution.

in Fig. 1(a).[41] Typically, a 200 nm thick silver layer was sputtered onto the membrane as the working electrode, and then silver, gold and iron segments were electrochemically deposited within the pores. After that, the membrane with the gold/iron nanorods inside was thermally annealed in order to convert iron to iron oxide, and the rods were then released by dissolving the membrane and sacrificial silver segment (for experimental details see the ESI† Materials and methods). Fig. 2(b) shows a scanning electron microscope (SEM) image of a gold/iron oxide nanorod. The diameter and the length of the nanorod are approximately 300 nm and 3 μm, respectively. The length ratio of the gold and iron oxide segments is approximately 1 : 1. Energy dispersive X-ray spectroscopy (EDS) mapping confirms the expected elemental composition. X-ray diffraction (XRD) patterns (ESI,† Fig. S1(b)) showed that the iron oxide segment contained mostly α-Fe_2O_3, which is an n-type semiconductor material that has been widely studied for photocatalytic water splitting.[42] X-ray photoelectron spectroscopy measurements (ESI,† Fig. S1(a)), however, indicated the existence of mixed oxidation states for iron, namely Fe^{2+} and Fe^{3+}, suggesting the possible presence of a magnetite (Fe_3O_4) phase. This material absorbs visible light of wavelengths shorter than ~500 nm, as measured by diffuse reflectance UV-vis in Fig. 1(c). We also measured the zeta potential of the gold/iron nanorods, which was -20 ± 1 mV.

When the gold/iron oxide nanorods were suspended in hydrogen peroxide solution (H_2O_2, 2.5 v%) and illuminated with a mercury lamp, autonomous motion was observed. The nanomotors move with the gold end trailing at a speed up to 30 μm s^{-1} at a light intensity of 33 mW mm^{-2}. The same nanorods show only Brownian motion when observed with dark field microscopy. A 380 nm UV filter was used to eliminate the contribution of UV light. As a first step towards understanding the visible light-driven propulsion, we set out to investigate the relative contributions of two possibly important factors in the experiment: the H_2O_2 concentration and the light intensity. We first measured the influence of H_2O_2 concentration on the speed of gold/iron oxide nanomotors, expecting an increase in the speed of motor with increasing H_2O_2 concentration, which is typical for chemically driven nanomotors.[19] Fig. 2(b) shows the measured speeds at a constant light intensity of 33 mW mm^{-2} (ESI,† Video S1). We observed that the gold/iron oxide nanomotors exhibited axial motion when the concentration of hydrogen peroxide was as low as 0.005 v%. The velocity increased with increasing concentration of H_2O_2, and above 0.1 v%, the concentration has a negligible effect. We also measured the motion of Au–Fe_2O_3 nanomotors in DI water without H_2O_2 and no obvious axial motion was observed. In contrast to the weak dependence of speed on H_2O_2 concentration, the light intensity has a significant effect on the speed of nanomotors. The light intensity was varied from 3.0 to 33 mW mm^{-2} through neutral density filters equipped on the microscope. Fig. 2(c) shows that the speed of a single gold/iron oxide nanorod in 2.5 v% H_2O_2 increases with increasing light intensity, reaching ~30 μm s^{-1} for a light intensity of 33 mW mm^{-2} (ESI,† Video S2). This indicates that the light intensity limits the speed of the gold/iron oxide nanomotors, so long as a minimal amount (0.10 v%) of H_2O_2 was present. Compared to bimetallic motors, which typically have a high background rate of catalytic decomposition of H_2O_2, the gold/iron oxide motors have relatively high fuel efficiency.[43]

By analogy to Cu_2O/Au and Si–Au micromotors, we postulated a propulsion mechanism based on light-induced self-electrophoresis. In this mechanism, electron–hole pairs are generated in the iron oxide and separated at the iron oxide/solution interface when the nanomotors are irradiated by visible light; electrons should be transferred to gold from n-type iron oxide because of the ohmic contact between the two materials, and holes should be driven to the iron oxide/solution interface by band bending.[44] As a result, reduction and oxidation of H_2O_2 should occur at the gold and iron oxide ends, respectively, leading to a proton concentration gradient around the rod. Consequently, the negatively charged nanorod should move towards the iron oxide, which is consistent with experimental observations.[19,45,46] We note that this mechanism is similar to that proposed by Hong *et al.* to explain the motion of TiO_2 microparticles in UV light,[45] except that in this case iron oxide has a narrower bandgap and can be excited by visible light.

To test the proposed mechanism, the mixed potentials of gold and iron oxide microelectrodes in 2.5 v% H_2O_2 solution with and without illumination were measured. The mixed potential of a catalytic metal in H_2O_2 indicates its tendency to preferentially catalyze the oxidation (more negative mixed potential) or the reduction (more positive mixed potential) of H_2O_2. This method has been widely used to characterize the electrochemical behavior of electrophoretically driven nanomotors.[46–49] As shown in the Tafel plots in Fig. 3(a), the difference in mixed potentials between gold and iron oxide electrodes is approximately 60 mV in the dark, but it increases to 140 mV when iron oxide is illuminated at a light density of 100 mW cm^{-2} (note: a different light source was used here than

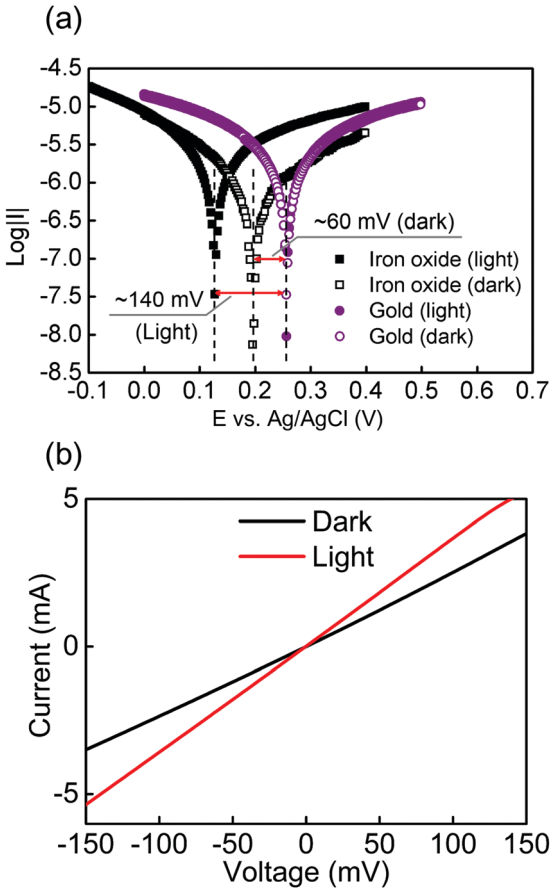

Fig. 3 (a) Tafel plot of iron oxide and gold electrodes with respect to Ag/AgCl reference electrode with and without illumination in 2.5 v% hydrogen peroxide solution. (b) *I–V* curve of a solid state gold/iron oxide junction electrode showing ohmic behavior.

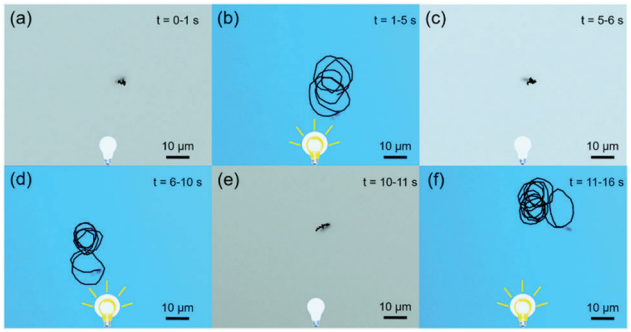

Fig. 4 (a–f) Time-lapse snapshots showing trajectories of a gold/iron oxide nanomotor in 2.5 v% hydrogen peroxide solution during light switching.

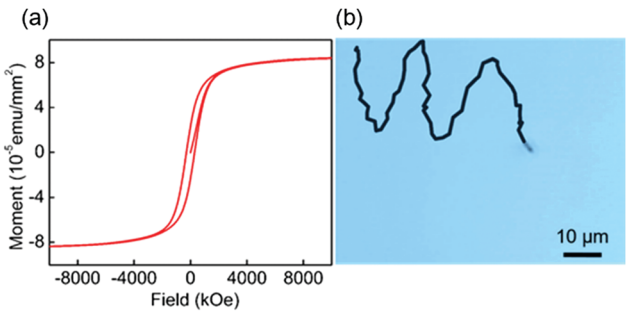

Fig. 5 (a) Magnetic moment of iron oxide nanorod measured by vibrating sample magnetometer. (b) Magnetic control of gold/iron oxide nanorod following specific trajectories in 2.5 v% hydrogen peroxide solution under mercury light of 33 mW mm^{-2}.

the mercury lamp used for propulsion experiments). This photovoltage effect is consistent with a light-induced oxidation reaction at the n-type Fe_2O_3/solution interface. Under illumination or in the dark, iron oxide is always found to have a more negative mixed potential than gold, indicating that electrons migrate from iron oxide to gold. This is consistent with the observation that the iron oxide segments are the leading ends of gold/iron oxide nanomotors.

To quantify the photoconductivity of the material, iron oxide was first electrochemically deposited onto a piece of fluorine doped tin oxide (FTO) glass, followed by thermal annealing.[40] After that, a 100 nm-thick gold film was sputtered onto the iron oxide. From the *I–V* plot of a gold/iron oxide solid junction (Fig. 3(b)) we can calculate that the resistance was 39.7 Ω without illumination and dropped to 26.7 Ω when the mercury lamp was turned on. This indicates a significant drop in resistivity under illumination. In addition, the linearity in the *I–V* plot indicates an ohmic contact between gold and iron oxide. Based on these electrochemical measurements we can conclude that the photovoltage and the photoconductivity induced by visible light are both factors in the motility of gold/iron oxide nanomotors.

Gold/iron oxide nanomotors show good external controllability. This can be demonstrated by their rapid go/stop motion using light switching (ESI,† Video S3). Fig. 4(a), (c) and (e) show that a gold/iron oxide nanomotor exhibits only Brownian motion in the absence of illumination, and immediately starts to move rapidly when the light is switched on (Fig. 4(b), (d) and (f)). This kind of fast response and on/off switching can be useful in a range of applications.[46] In addition, the ability to steer nanomotors is useful. Because the iron oxide segments are superparamagnetic (Fig. 5(a)), the nanomotors can be readily aligned and steered by external magnetic fields (Fig. 5(b) and ESI,† Video S4). Typically, magnetic steering is introduced into rod-like nanomotors by the incorporation of ferromagnetic Ni segments; however the presence of ferromagnetic segments causes aggregation of the rods, which can be avoided by using superparamagnetic nanoparticles. An additional advantage of superparamagnetic motors is their ability to navigate along magnetic field lines.[50] We do not observe any aggregation of the nanomotors in the dark, although some reversible dimerization events – which are likely the result of catalytically generated electric fields[51] – were observed under illumination.

In conclusion, rod-like gold/iron oxide nanomotors were synthesized in AAO membranes by electrochemical deposition. The nanomotors could be activated by visible light at very low concentrations of hydrogen peroxide, and their speed can be modulated by the light intensity. The propulsion mechanism is light-induced self-electrophoresis in which the photovoltage and photoconductivity both affect the velocity. The presence

of superparamagnetic particles in the iron oxide segments enables steering with external magnetic fields. The key characteristics of these nanomotors include inexpensive and scalable synthesis, fast propulsion at low concentrations of chemical fuels, visible light operation, on/off switching and magnetic steerability, all of which are useful features for potential applications.

This work was supported by the National Science Foundation under MRSEC grant number DMR-1420620. D. Zhou, G. Zhang and L. Li are grateful for the financial support from the National Natural Science Foundation of China (51522003 and 51175129), Key Laboratory of Micro-systems and Microstructures Manufacturing of Ministry of Education (2016KM004), Program of Introducing Talents of Discipline to Universities (Grant No. B07018) and Self-Planned Task of State Key Laboratory of Robotics and System (HIT) (SKLRS201706A)

Conflicts of interest

There are no conflicts to declare.

Notes and references

1 T. E. Mallouk and A. Sen, *Sci. Am.*, 2009, **300**, 72–77.
2 J. Wang, *ACS Nano*, 2009, **3**, 4–9.
3 S. Tottori, L. Zhang, F. Qiu, K. K. Krawczyk, A. Franco-Obregón and B. J. Nelson, *Adv. Mater.*, 2012, **24**, 811–816.
4 D. Kagan, M. J. Benchimol, J. C. Claussen, E. Chuluun-Erdene, S. Esener and J. Wang, *Angew. Chem., Int. Ed.*, 2012, **51**, 7519–7522.
5 S. Ahmed, W. Wang, L. O. Mair, R. D. Fraleigh, S. Li, L. A. Castro, M. Hoyos, T. J. Huang and T. E. Mallouk, *Langmuir*, 2013, **29**, 16113–16118.
6 X. Ma, K. Hahn and S. Sanchez, *J. Am. Chem. Soc.*, 2015, **137**, 4976–4979.
7 K. Kim, J. Guo, X. Xu and D. L. Fan, *Small*, 2015, **11**, 4037–4057.
8 G. A. Ozin, I. Manners, S. Fournier-Bidoz and A. Arsenault, *Adv. Mater.*, 2005, **17**, 3011–3018.
9 S. Campuzano, D. Kagan, J. Orozco and J. Wang, *Analyst*, 2011, **136**, 4621–4630.
10 X. Xu, H. Li, D. Hasan, R. S. Ruoff, A. X. Wang and D. L. Fan, *Adv. Funct. Mater.*, 2013, **23**, 4332–4338.
11 M. S. Hanay, S. Kelber, A. K. Naik, D. Chi, S. Hentz, E. C. Bullard, E. Colinet, L. Duraffourg and M. L. Roukes, *Nat. Nanotechnol.*, 2012, **7**, 602–608.
12 S. Ahmed, D. T. Gentekos, C. A. Fink and T. E. Mallouk, *ACS Nano*, 2014, **8**, 11053–11060.
13 M. Ibele, T. E. Mallouk and A. Sen, *Angew. Chem., Int. Ed.*, 2009, **48**, 3308–3312.
14 W. Wang, W. Duan, A. Sen and T. E. Mallouk, *Proc. Natl. Acad. Sci. U. S. A.*, 2013, **110**, 17744–17749.
15 L. Soler and S. Sanchez, *Nanoscale*, 2014, **6**, 7175–7182.
16 J. Orozco, V. García-Gradilla, M. D'Agostino, W. Gao, A. Cortés and J. Wang, *ACS Nano*, 2013, **7**, 818–824.
17 W. Gao, X. Feng, A. Pei, Y. Gu, J. Li and J. Wang, *Nanoscale*, 2013, **5**, 4696–4700.
18 M. Guix, J. Orozco, M. García, W. Gao, S. Sattayasamitsathit, A. Merkoçi, A. Escarpa and J. Wang, *ACS Nano*, 2012, **6**, 4445–4451.
19 W. F. Paxton, K. C. Kistler, C. C. Olmeda, A. Sen, S. K. St. Angelo, Y. Cao, T. E. Mallouk, P. E. Lammert and V. H. Crespi, *J. Am. Chem. Soc.*, 2004, **126**, 13424–13431.
20 M. Pumera, *Nanoscale*, 2010, **2**, 1643–1649.
21 P. Fischer and A. Ghosh, *Nanoscale*, 2011, **3**, 557–563.
22 A. Ghosh and P. Fischer, *Nano Lett.*, 2009, **9**, 2243–2245.
23 T. Li, J. Li, H. Zhang, X. Chang, W. Song, Y. Hu, G. Shao, E. Sandraz, G. Zhang, L. Li and J. Wang, *Small*, 2016, **12**, 6098–6105.
24 P. Calvo-Marzal, S. Sattayasamitsathit, S. Balasubramanian, J. R. Windmiller, C. Dao and J. Wang, *Chem. Commun.*, 2010, **46**, 1623–1624.
25 S. T. Chang, V. N. Paunov, D. N. Petsev and O. D. Velev, *Nat. Mater.*, 2007, **6**, 235–240.
26 W. Wang, L. A. Castro, M. Hoyos and T. E. Mallouk, *ACS Nano*, 2012, **6**, 6122–6132.
27 W. Wang, S. Li, L. Mair, S. Ahmed, T. J. Huang and T. E. Mallouk, *Angew. Chem., Int. Ed.*, 2014, **53**, 3201–3204.
28 V. Garcia-Gradilla, J. Orozco, S. Sattayasamitsathit, F. Soto, F. Kuralay, A. Pourazary, A. Katzenberg, W. Gao, Y. Shen and J. Wang, *ACS Nano*, 2013, **7**, 9232–9240.
29 A. L. Balk, L. O. Mair, P. P. Mathai, P. N. Patrone, W. Wang, S. Ahmed, T. E. Mallouk, J. A. Liddle and S. M. Stavis, *ACS Nano*, 2014, **8**, 8300–8309.
30 H.-R. Jiang, N. Yoshinaga and M. Sano, *Phys. Rev. Lett.*, 2010, **105**, 268302.
31 L. Baraban, R. Streubel, D. Makarov, L. Han, D. Karnaushenko, O. G. Schmidt and G. Cuniberti, *ACS Nano*, 2013, **7**, 1360–1367.
32 R. A. Pavlick, S. Sengupta, T. McFadden, H. Zhang and A. Sen, *Angew. Chem., Int. Ed.*, 2011, **50**, 9374–9377.
33 J. Wang, Z. Xiong, X. Zhan, B. Dai, J. Zheng, J. Liu and J. Tang, *Adv. Mater.*, 2017, **29**, 1701451.
34 Y. Wu, R. Dong, Q. Zhang and B. Ren, *Nano-Micro Lett.*, 2017, **9**, 30.
35 Q. Zhang, R. Dong, Y. Wu, W. Gao, Z. He and B. Ren, *ACS Appl. Mater. Interfaces*, 2017, **9**, 4674–4683.
36 F. Wong and A. Sen, *ACS Nano*, 2016, **10**, 7172–7179.
37 B. Jang, A. Hong, H. E. Kang, C. Alcantara, S. Charreyron, F. Mushtaq, E. Pellicer, R. Büchel, J. Sort, S. S. Lee, B. J. Nelson and S. Pané, *ACS Nano*, 2017, **11**, 6146–6154.
38 R. Dong, Y. Hu, Y. Wu, W. Gao, B. Ren, Q. Wang and Y. Cai, *J. Am. Chem. Soc.*, 2017, **139**, 1722–1725.
39 X. Lin, T. Si, Z. Wu and Q. He, *Phys. Chem. Chem. Phys.*, 2017, **19**, 23606–23613.
40 D. Zhou, Y. C. Li, P. Xu, N. S. McCool, L. Li, W. Wang and T. E. Mallouk, *Nanoscale*, 2017, **9**, 75–78.
41 A. Mao, G. Y. Han and J. H. Park, *J. Mater. Chem.*, 2010, **20**, 2247–2250.
42 A. G. Tamirat, J. Rick, A. A. Dubale, W.-N. Su and B.-J. Hwang, *Nanoscale Horiz.*, 2016, **1**, 243–267.
43 W. Wang, T.-Y. Chiang, D. Velegol and T. E. Mallouk, *J. Am. Chem. Soc.*, 2013, **135**, 10557–10565.
44 A. G. Tamirat, J. Rick, A. A. Dubale, W. N. Su and B. J. Hwang, *Nanoscale Horiz.*, 2016, **1**, 243–267.
45 Y. Hong, M. Diaz, U. M. Córdova-Figueroa and A. Sen, *Adv. Funct. Mater.*, 2010, **20**, 1568–1576.
46 R. Dong, Q. Zhang, W. Gao, A. Pei and B. Ren, *ACS Nano*, 2016, **10**, 839–844.
47 Y. Wang, R. M. Hernandez, D. J. Bartlett, J. M. Bingham, T. R. Kline, A. Sen and T. E. Mallouk, *Langmuir*, 2006, **22**, 10451–10456.
48 U. K. Demirok, R. Laocharoensuk, K. M. Manesh and J. Wang, *Angew. Chem., Int. Ed.*, 2008, **47**, 9349–9351.
49 Q. Xiao, J. Li, J. Han, K.-X. Xu, Z.-X. Huang, J. Hu and J.-J. Sun, *RSC Adv.*, 2015, **5**, 71139–71143.
50 P. Dhar, Y. Cao, T. Kline, P. Pal, C. Swayne, T. M. Fischer, B. Miller, T. E. Mallouk, A. Sen and T. H. Johansen, *J. Phys. Chem. C*, 2007, **111**, 3607–3613.
51 W. Wang, W. Duan, A. Sen and T. E. Mallouk, *Proc. Natl. Acad. Sci. U. S. A.*, 2013, **110**, 11744–11749.

